Structure of the His44 → Ala Single Point Mutant of the Distal Finger Motif of HIV-1 Nucleocapsid Protein: A Combined NMR, Molecular Dynamics Simulation, and Fluorescence Study†

Roland H. Stote,*,‡,⊗ Esther Kellenberger,#,||,⊗ Hervé Muller,‡ Elisa Bombarda,§ Bernard P. Roques,⊥ Bruno Kieffer,# and Yves Mély*,§

Laboratoire de Chimie Biophysique, ISIS UMR 7006 CNRS, Université Louis Pasteur, 8 allée Gaspard Monge, BP 70028, F-67083 Strasbourg Cedex, France, Laboratoire de Biologie et de Génomique Structurales, Groupe de RMN, UMR 7104 CNRS, ESBS, bd Sebastien Brant, 67400 Illkirch, France, Laboratoire de Pharmacochimie Moléculaire et Structurale INSERM U266 − CNRS FRE 2463, Faculté de Pharmacie, 4 avenue de l'Observatoire, 75006 Paris, France, and Laboratoire de Pharmacologie et Physico-Chimie des Interactions Cellulaires et Moléculaires, UMR 7034 CNRS, Faculté de Pharmacie, 74, Route du Rhin, 67401 Illkirch, France

Received November 27, 2003; Revised Manuscript Received March 29, 2004

ABSTRACT: The nucleocapsid protein (NCp7) of human immunodeficiency virus type 1 (HIV-1) contains two highly conserved CCHC zinc fingers that strongly bind Zn^{2+} through coordination of one His and three Cys residues. It has been suggested that NCp7 function is conformation specific since substitution of any of the zinc coordinating residues in the zinc finger motifs leads to subsequent loss of viral infectivity. To further determine the structural requirements necessary for this specific conformation, we investigated by ^{1}H 2D NMR and molecular dynamics simulations the structure of the distal finger motif of NCp7 in which the zinc coordinating amino acid, His 44, was substituted by a noncoordinating Ala residue. While the fold of the N-terminal part of this mutated peptide was similar to that of the native peptide, an increased lability and significant conformational changes were observed in the vicinity of the His-to-Ala mutation. Moreover, molecular dynamics simulations suggested a mechanism by which the variant peptide can bind zinc ion even though one zinc-coordinating amino acid was lacking. Using the fluorescence of the naturally occurring Trp37 residue, the binding affinity of the variant peptide to the $(TG)_3$ model oligonucleotide was found to be decreased by about 2 orders of magnitude with respect with the native peptide. Modeling of the DNA:NCp7 complex using structures of the variant peptide suggests that the residues forming a hydrophobic cleft in the native protein are improperly oriented for efficient DNA binding by the variant peptide.

The nucleocapsid proteins are small, highly basic proteins generated by processing of the Gag polyproteins during retrovirus maturation. With the exception of spumaretroviruses (*1*, *2*), the retroviral nucleocapsid proteins contain one or two copies of a zinc finger motif characterized by the sequence $C-X_2-C-X_4-H-X_4-C$ (X being a variable amino acid residue) and thus also called the CCHC motif (*3*). In human immunodeficiency virus type 1 (HIV-1),[1] the nucleocapsid protein NCp7 is characterized by two CCHC motifs that bind Zn^{2+} with very high affinity ($10^{13}-10^{14}$ M^{-1}) (*4*, *5*). Binding of Zn^{2+} results in a conformational change from a flexible unfolded state to a highly constrained folded structure in which the two CCHC motifs of NCp7 (*6*−*8*) are very similar. In addition, due to the kink induced by Pro^{31} in the linker sequence between the two finger motifs, these latter are thought to be spatially close and weakly interacting with one another (*7*−*10*).

Coordination of Zn^{2+} has been shown to be necessary for most NCp7 functions since potential antiviral agents that disrupt the zinc binding motifs by ejecting Zn^{2+} (*4*, *11*, *12*) and mutations that prevent Zn^{2+} binding lead to noninfectious viruses (*13*−*17*). This may be partly due to the inability of disrupted or mutated NCp7 sequences in the Gag polyproteins to selectively recognize and package genomic RNA into new virus particles (*8*, *13*−*22*). However, since these finger motif disruptions or mutations lead to a much greater

† This work was supported by the Centre National de la Recherche Scientifique (CNRS) and by grants from the Agence Nationale de Recherches sur le Sida (ANRS) and SIDACTION (Ensemble contre le Sida) and the European Community (TRIoH integrated project). Support from the Région Alsace is gratefully acknowledged.

* Corresponding authors: R. Stote, rstote@isis.u-strasbg.fr; Y. Mély, mely@aspirine.u-strasbg.fr.

⊗ These authors should be considered joint first authors.

‡ ISIS UMR 7006 CNRS.

Laboratoire de Biologie et de Génomique Structurales, UMR 7104 CNRS.

⊥ Laboratoire de Pharmacochimie Moléculaire et Structurale INSERM U266 − CNRS FRE 2463.

§ Laboratoire de Pharmacologie et Physico-Chimie des Interactions Cellulaires et Moléculaires, UMR 7034 CNRS.

|| Current address: Bioinformatics Group UMR 7081, Faculté de Pharmacie, 74 route du Rhin, BP24, F-67401 Illkirch Cedex, France.

[1] Abbreviations: HIV-1, human immunodeficiency virus type 1; NCp7 nucleocapsid protein of HIV-1; NC nucleocapsid protein; NOE, nuclear overhauser effect; NOESY, NOE spectroscopy; COSY correlated spectroscopy; TOCSY, total correlated spectroscopy; RMS, root-mean-square; RMSD, root-mean-square deviation.

10.1021/bi036137u CCC: $27.50
Published on Web 05/22/2004

defect in infectivity than in genome packaging, it is likely that Zn^{2+} coordination is also required for other NCp7 functions. In fact, an increasing amount of evidence shows that Zn^{2+} coordination is also required for the nucleic acid chaperone activity of NCp7, especially during the reverse transcription steps (*23*−*30*). Although Zn^{2+} coordination to the finger motifs is necessary for function, accumulating evidence suggests that it is not sufficient. Indeed, substitution of one of the CCHC motifs by either a CCHH or CCCC motif, mutations that do not prevent binding of Zn^{2+} but induce a different conformational arrangement around the Zn^{2+} ion (*31*, *32*), also lead to noninfectious viruses (*22*, *31*, *33*, *34*). As when Zn^{2+} is absent, the non-native conformations in the mutated zinc finger motifs of NCp7 hamper selective recognition of genomic RNA and induce defective reverse transcription and integration (*22*, *28*, *31*, *33*−*35*). A similar phenotype is obtained when one of the Zn^{2+}-coordinating residue is substituted by a noncoordinating one (*15*). Recent investigations have shown that although the binding constants of these mutants for Zn^{2+} are significantly reduced as compared to the native protein, they remain similar to other Zn^{2+} binding proteins (*36*). Among the four Zn^{2+}-coordinating residues of the distal finger motif of NCp7, the substitution of His44 by an Ala residue is found to induce the smallest decrease in the binding constant. Moreover, this mutation still permits the tetrahedral coordination of the metal ion with the vacant ligand position presumably occupied by a water molecule. This suggests that loss of viral infectivity is not related to the loss of Zn^{2+} binding (*5*).

To further explore the structure−activity relationship for HIV zinc finger motifs, ^{1}H NMR and molecular modeling were used to investigate the structural changes induced by the substitution of His 44 by a non-zinc-coordinating Ala residue in the HIV distal finger motif. The present work shows that the three-dimensional structure of Ala44:NC(35−50) peptide is different from that of the CCCC or CCHH mutants, being characterized by high flexibility especially for the residues close to the mutated position. This high flexibility leads to an ensemble of conformations in which the hydrophobic cleft that is critical for interaction of NCp7 with nucleic acids is not formed. This, in turn, explains the significant decrease in affinity of Ala44:NC(35−50), with respect to the native (35−50)NCp7 peptide, for an oligonucleotide model. These findings are relevant for both finger motifs of NC since the folding of these motifs is highly similar and since mutations of the zinc coordinating residues in both finger motifs induce similar infectivity losses.

MATERIALS AND METHODS

NMR Measurements and Structure Calculation. The Ala44:NC(35−50) peptide, prepared by solid-phase synthesis (*37*) was dissolved in argon-degassed 90% H_2O/10% D_2O to give a final concentration of 1 mM. $ZnCl_2$ was added in 1.1-fold excess with respect to the peptide concentration. pH was adjusted to 6.5 at room temperature. Two-dimensional ^{1}H experiments were collected at 274 K with a Bruker DRX-600. COSY, TOCSY (80 ms mixing time), and NOESY (three different mixing times: 50, 200, and 400 ms) spectra were recorded with 2K real points in t2 with a spectral width of 7002 Hz and 512 t1 increments. In all experiments, the water signal was suppressed using a WATERGATE sequence (*38*). The data were processed using the UXNMR software (Bruker). A $\pi/2$ phase-shifted sine bell window function was applied prior to Fourier transformation in both dimensions. The final size of the matrixes was 2K × 1K real points.

Spectra analysis was carried out using the XEASY program (*39*). Experimental interproton distance restraints based on NOE cross-peaks (mixing time of 200 ms) were obtained by classifying peak volumes as strong, medium, and weak, corresponding to upper distances of 2.5, 3.2, and 4.5 Å, respectively.

Two sets of 50 structures were generated using the restrained simulated annealing protocol implemented in the program X-PLOR 3.851 (*40*) starting from extended conformations. The first calculation was performed using only NOE distances as experimental restraints, whereas the second one included three additional Sγ-Zn distance restraints. The structures of the second set were further refined using a slow cooling restrained simulated annealing protocol (*41*). The 18 best structures were then chosen based on the following selection criteria: good geometry, no NOE violations greater than 0.3 Å.

Visualization and superposition of the structures were performed using the MolMol program (*42*). The angular order parameters were calculated using an in-house program.

Molecular Dynamics Simulations. Three molecular dynamics simulations of the Ala44:NC(35−50) peptide were done using explicit solvent and periodic boundary conditions. The initial coordinates for the simulations were obtained from the native structure of the NCp7(12−53) protein of HIV-1 determined by Morellet et al. (*7*, *8*) by solution NMR spectroscopy. For each simulation, a different structure from the NMR ensemble was used. The amino acids prior in sequence to Gly35, and after Thr50, were deleted, leaving only residues 35−50 of the C-terminal zinc finger. The point mutation His44-to-Ala was introduced by replacing His44 by an Ala residue while keeping the same orientation. The CHARMM program (*43*) and the CHARMM all-atom protein parameter (*44*) set were used for all calculations. All Cys residues were in the deprotonated state, consistent with experimental results (*5*). The following protocol was used: the protein was solvated by a 31.1 Å side length box of TIP3P water; counterions were added to neutralize the overall charge of the protein to obtain a neutral system. Four additional NaCl ions pairs were randomly distributed around the protein. Between 886 and 893 water molecules were added to the system giving a total of 2898 or 2919 atoms, respectively. A 13 Å nonbond list was used with the SHIFT cutoff function for the electrostatics and the SWITCH cutoff function for the van der Waals interactions. The water was initially equilibrated around the fixed protein for 10 ps at 300 K. The constraints on the protein were removed and the system was energy minimized for 100 steps of steepest descent minimization. Initial velocities were assigned at 150 K and the system was heated to 300 K, the temperature of the simulations. The three simulations were done for 4.7, 5.6, and 6 ns. All molecular dynamics simulations were calculated on an Origin3800.

An average structure was calculated over every 25 ps segment of the simulations. Global rotation was removed by superposing the N- and C-terminal residues (residues 36:41 and 38:50, respectively) and minimizing their RMS difference. This follows the same procedure used to reorient

and superimpose the NMR structures, thus allowing a comparison to the NMR structures. From these average structures, the RMS fluctuations averaged by residue were calculated. The structures determined by NMR and the structures from the molecular dynamics simulations were used to calculate chemical shifts to compare to the experimental data. Chemical shift data contain information of local conformations that can be useful for validating and refining structures. The empirical model developed by Ösapay and Case (*45*, *46*) was used to calculate the proton chemical shifts in Ala44:NC(35−50). This model calculates the difference in proton chemical shifts between random coil and folded conformations of proteins and has been shown to give satisfactory results for carbon-attached protons, but the results for nitrogen-attached hydrogens are not as satisfying (*45*). For that reason, we only compared carbon-attached hydrogens between the different structures. Each of the average structures calculated from the simulations were used to calculate the chemical shifts and an overall average difference from experiment was calculated.

The average interproton distance, R, was calculated for each configuration in the production phase of the simulation using the formula:

$$R = \langle r^{-6} \rangle^{-1/6} \tag{1}$$

where the brackets indicate an average over all conformations. Ambiguous NOEs were considered satisfied if one of the two proton pairs satisfied the distance constraint.

The ART-2 algorithm implemented in the CHARMM program (*47*) was used to cluster all the structures from the molecular dynamics trajectories based on their backbone dihedral angles. Average structures representing each cluster were calculated.

Fluorescence Measurements and Titrations. Fluorescence titrations and anisotropy measurements were performed at 293 K on a SLM48000 spectrofluorometer. Excitation and emission wavelengths were 295 and 350 nm, respectively. Fluorescence titrations were performed by adding increasing oligonucleotide concentrations to a fixed amount of peptide, in 50 mM Hepes, 0.1 M NaCl, pH 7.5. Fluorescence intensities were corrected for dilution, buffer fluorescence, and screening effects due to the presence of nucleic acid. The average number ν, of moles of peptide bound per mole of oligonucleotide, is calculated from the fluorescence intensities using

$$\nu = (I_0 - I)/(I_0 - I_t)xL_t/N_t \tag{2}$$

where L_t and N_t designate the total concentration of peptide and oligonucleotide, respectively, I_t is the fluorescence at the plateau when all the peptide is bound, and I_0 and I correspond to the fluorescence intensities of the peptide in the absence and in the presence of a given concentration of oligonucleotide, respectively. Furthermore, the free peptide concentration, L, is deduced by $L = L_t - \nu N_t$. Since the affinity of the peptides was rather low, the plateau of fluorescence, I_t, could not be determined experimentally and was therefore calculated from a nonlinear fit of the following equation:

$$I = I_0 - \frac{(I_0 - I_t)}{L_t} x \frac{(1 + (L_t + nN_t)K_{obs}) - \sqrt{(1 + (L_t + nN_t)K_{obs})^2 - 4L_t nN_t K_{obs}^2}}{2K_{obs}} \tag{3}$$

where K_{obs} corresponds to the observed binding constant. The number, n, of peptide binding sites was taken to be 1.

RESULTS

NMR. (a) Ala44:NC(35−50) Assignment. The solution structure of the Ala44:NC(35−50) mutant peptide at pH 6.5 in the presence of an excess of zinc was investigated by proton NMR. One-dimensional spectra recorded at room temperature revealed broad resonances that are likely due to conformational exchange that occurs in the peptide. Improvement of the spectrum quality was obtained by decreasing the temperature down to 274 K. Therefore, Ala44:NC(35−50) structural study was performed at this temperature.

Sequence specific assignment was carried out by standard methods using COSY, TOCSY, and NOESY spectra. The TOCSY fingerprint of Ala44:NC(35−50) peptide is shown in Figure 1. This spectrum shows that the signals arising from the different amino acid spin systems are well resolved. However, additional peaks corresponding to a minor conformation are also present. As judged from relative Hα-HN cross-peak intensities, this minor conformation represents less than 10% of the population. In particular, this minor conformation is clearly observed for the spin system of Thr50 by the presence of exchange cross-peaks in the TOCSY spectrum (Figure 1). Exchange cross-peaks were only observed for the C-terminal residues, for which peak intensities of both major and minor conformations were 3−4 times higher than for the rest of the peptide. A minor conformation could also be deduced for Cys49 from sequential connectivities on the NOESY spectrum. Although no further sequential NOE between minor peaks could be observed, it appears that the backbone of the eight C-terminal residues, including the mutated alanine, experience conformational exchange. The aliphatic region of spectra revealed that Lys38 side chain also adopts several conformations, one of them being more populated than the others. All backbone and side chain resonances were unambiguously assigned for the major conformation. The complete proton assignment is reported in Table 1.

(b) Ala44:NC(35−50) Is Partially Folded and Binds Zinc. The chemical shift dispersion observed for Ala44:NC(35−50) indicates that the peptide adopts a folded conformation in the presence of zinc. For instance, the Cys39 amino proton frequency (7.65 ppm) differs significantly from the expected "random coil" values (8.6−7.8 ppm). The qualitative interpretation of interresidue NOE data (Figure 2) also supports the conclusion that Ala44:NC(35−50) is structured in solution. Four long range connectivities indicate that the N-terminus is close to the C-terminus. In particular, NOEs were observed between Trp37 side chain and Thr50 Hα, and between the side chains of (Trp37−Asp48) and (Lys38−Cys49) couples. Another five medium and long-range NOEs were observed within the Cys36−Lys41 fragment, suggesting

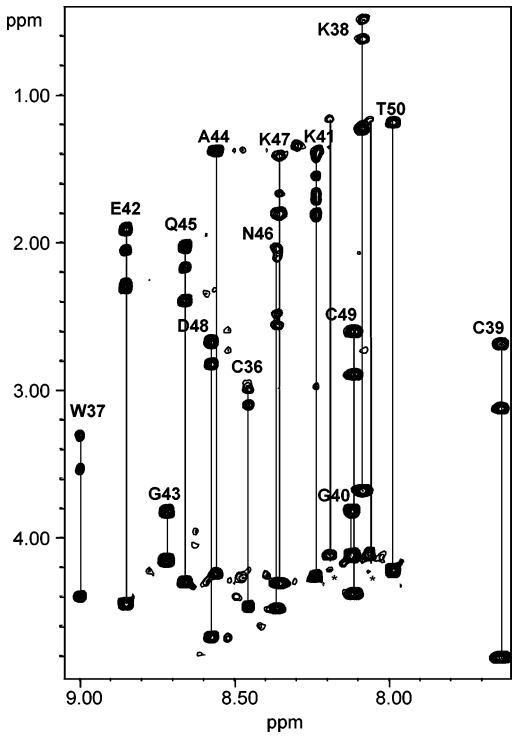

FIGURE 1: Fingerprint of the TOCSY spectrum of Ala44:NC(35−50) at pH 6.5 and 274 K. The spectra were calibrated using an external sample of 2,2-dimethyl-2-silapentane-5-sulfonate (DSS). Dotted lines denote two minor conformations for Thr50. Exchange cross-peaks between HN of Thr50 in minor conformations and Hα of Thr50 in the major conformation are shown with stars (∗).

Table 1: ^{1}H NMR Chemical Shift (ppm) of Ala44:NC(35−50) in H_2O at pH 6.5 and 274 K

residue	HN	Hα	Hβ	others			
G35		3.55−3.84					
C36	8.46	4.48	3.12-3.02				
W37	9.00	4.41	3.33-3.55	Hδ1	7.59	Hε3	7.51
				Hε1	10.32	Hζ3	7.14
				Hζ2	7.44	Hη2	7.23
K38	8.09	3.69	1.24	Hγ	0.52	Hδ	1.35
				Hε	2.75		
C39	7.65	4.82	2.71−3.13				
G40	8.13	3.84−4.13					
K41	8.24	4.27	1.73−1.83	Hγ	1.43−1.57		
				Hδ	1.68	Hε	2.65
E42	8.86	4.46	1.93−2.07	Hγ	2.31		
G43	8.72	3.83−4.16					
A44	8.54	4.26	1.40				
Q45	8.67	4.31	2.05−2.18	Hγ	2.41	Hε	7.26−7.68
M46	8.37	4.49	2.06−2.12	Hγ	2.50−2.58		
K47	8.37	4.32	1.70−1.82	Hγ	1.43	Hδ	1.69
				Hε	2.99		
D48	8.58	4.68	2.69−2.84				
C49	8.12	4.39	2.62−2.91				
T50	8.00	4.23	4.29	Hγ2	1.21		

that a short turn brings Cys36 and Cys39 cysteines in close vicinity. In the peptide fragment spanning from Ala44 to Lys47, the lack of short-range NOE is suggestive of local flexibility.

Using NOE data as distance restraints, structure calculations were carried out to further characterize the Ala44:NC(35−50) fold. A first set of 50 structures were generated by simulated annealing using 77 distance restraints and excluding the zinc ion. The subsequent analysis of side chains positions clearly indicated that the three cysteine residues are involved in zinc binding. A second set of 50 structures

FIGURE 2: Experimental restraints based on NOE connectivities A total of 77 NOE connectivities are distributed into 18 intraresidues and 59 interresidues restraints (49 sequential, four medium range, and six long range). Peak classification as strong, medium, and weak is specified by the thickness of the lines. The star (∗) indicates the His−Ala mutation position. (A) Relative intensities of four medium range (between amino acids i and i+[1−4]) and 29 sequential cross-peaks. Ni, αi, and βi represent amide, α- and β-protons of amino acid i, respectively. (B) Amino acids involved in the six observed long range (between amino acids i and i+[>4]) connectivities.

was then calculated for the peptide with zinc. Zinc coordination was fixed by setting the distance between zinc and cysteine Sγ atoms to 2.3 Å. The 18 best structures are shown in Figure 3A. They all satisfy the set of restraints within experimental error (no interproton distance violations greater than 0.3 Å and average RMSD of NOE restraints equal to 0.029 ± 0.001 Å) and display small deviation from idealized covalent geometry (the average RMSD are 0.0025 ± 0.0009 Å, 0.36 ± 0.08° and 0.25 ± 0.1° for bonds, angles, and impropers, respectively). The average final total energy is 18 ± 10 kcal/mol.

The atomic RMSD distribution of the individual structures about the mean coordinate position is 1.9 ± 0.4 Å for the backbone atoms. It decreases to 1.2 ± 0.6 Å if only residues 35−41 and 48−50 are considered (Figure 3B), indicating that the relative position of the N- and the C-terminal parts of the peptide is reasonably well defined.

Variations in angular order parameters indicate that only fragment 36−41 is internally well defined. These findings are consistent with the lack of experimental restraints in the region surrounding the mutation and also with the internal mobility revealed by the observation of exchange peaks in the NMR spectra.

The experimental structure of Ala44:NC(35−50) determined by the present NMR studies was compared to the experimental structure of the native C-terminal finger of the NCp7 protein (representative model from the Protein Data Bank entry 1ESK). A best-fit superposition of all backbone heavy atoms of the mutant peptide structure to those of the wild type resulted in a good overlap of both the zinc ion and the cysteines side chain positions (an RMSD of 1.7 ± 0.4 Å for Cβ, Sγ, and Zn atoms) even though the overall RMSD for the backbone heavy atoms was rather poor (3.8 ± 0.4 Å) (Figure 3C, left). A best-fit superposition of the backbone atoms of residues Gly35−Gly40 (N-terminal end) of both peptides yields a much better RMSD value, namely, 1.4 ± 0.2 Å. In this latter orientation (Figure 3C, right), the position of the metal ion binding site with respect to the backbone position of the N-terminal in Ala44:NC(35−50) is different from that observed in the wild-type peptide; the zinc atom is shifted in the former case by about 3.4 Å. The comparison shows that the N-terminal end encompassing the first two cysteines is not affected by the mutation, although the zinc ion is displaced. In contrast, the C-terminal part

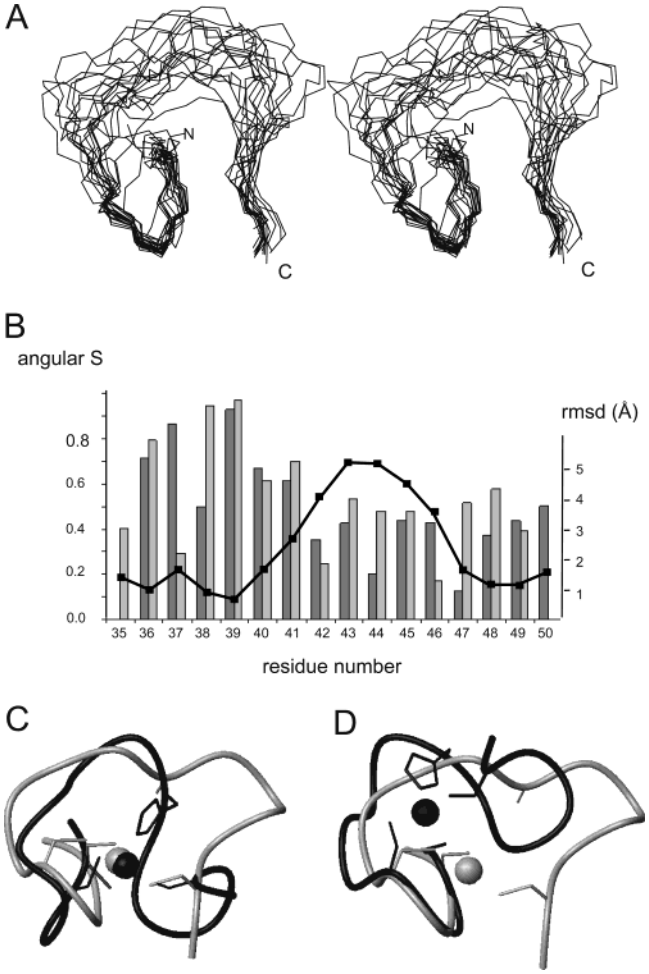

FIGURE 3: Ala44:NC(35−50) NMR structures. (A) Stereoview of Ala44:NC(35−50) NMR ensemble showing Cα, C, and N backbone atoms. Best-fit superposition of the backbone heavy atoms of Gly35−Lys41 and Asp48−Thr50 residues in the 18 conformers used to represent the structure. (B) Angular order parameter *S* and RMSD as a function of sequence. Angular order parameters *S* were calculated for psi (light gray bars) and phi (dark gray bars) Ala44:NC(35−50) angles. An *S* value close to zero means that the angle distribution in the structure ensemble is random whereas an *S* value equal to 1 characterizes a rigid torsion angle. The black curve indicates the RMSD from the average structure for the Ala44:NC(35−50) ensemble (best-fit superposition of backbone heavy atoms of residues Gly35−Lys41 and Asp48−Thr50). RMSD were calculated for the backbone heavy atoms. (C−D) Superposition of Ala44:NC(35−50) (black) and wild-type NC(35−50) (grey) structures (PDBID: 1ESK). Displayed are peptide backbones, side chains of Ala, His, and Cys residues and zinc ions. The average NMR structure of Ala44:NC(35−50) was fitted to a representative conformer of the native protein (PDB entry 1ESK) using the backbone heavy atoms of either residues 35:50 (C) or residues 35:40 (D).

(between residues 44 and 49) is strongly perturbed by the His:Ala mutation leading to a local unfolding of the polypeptide chain.

Molecular Dynamics Simulations. Although the NMR data are consistent with previous fluorescence spectroscopy results showing that the Ala44:NC(35−50) mutant is able to bind zinc ions (*36*), no detailed picture of the zinc coordination was obtained from the NMR data. To gain further insight into the structure and dynamics of the peptide and more specifically into the zinc coordination, molecular dynamics simulations were done.

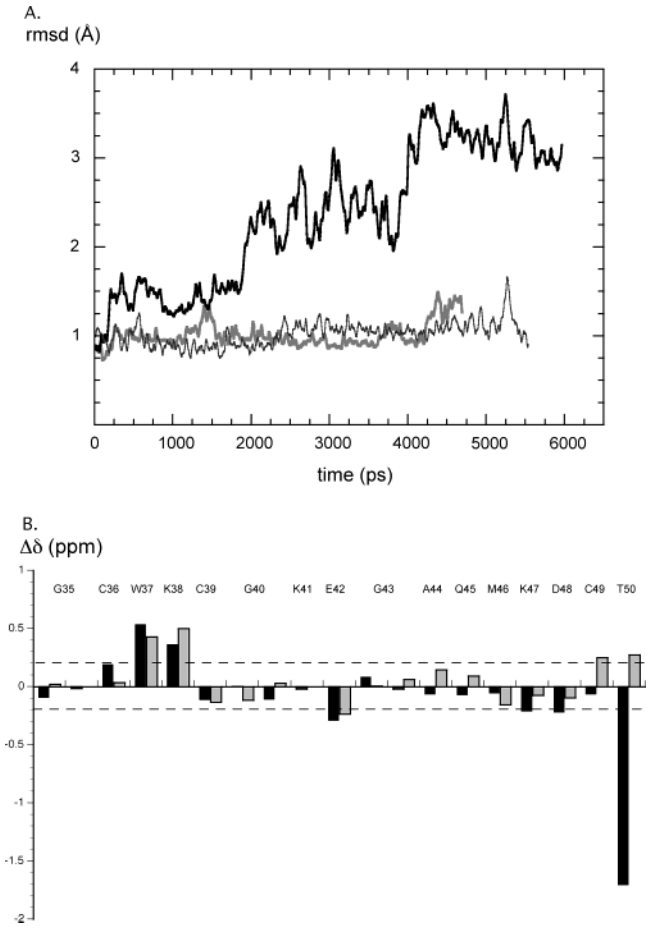

FIGURE 4: (A) Time series of RMSD values for the backbone atoms of the Ala44:NC(35−50) peptide from the molecular dynamics simulations. The RMSD was calculated for every coordinate set in the trajectory relative to the initial conformation and a running average of every 20 data points was plotted. The results are given individually for the three simulations. (B) Differences in the Hα chemical shifts between the experimental values and the values calculated using the NMR structures (black bar) and the average values from the simulation structures (grey bar). The dashed lines represent the estimated accuracy of the theoretical model used for the chemical shift calculations.

(a) Molecular Dynamics Simulations Confirm that Ala44:NC(35−50) Binds Zinc Ion. The backbone RMS coordinate difference (RMSD) from the initial structure, excluding the N- and C-terminal residues, were calculated from three molecular dynamics simulations as a function of time; the time series are shown in Figure 4A. Each configuration in the simulation was reoriented with respect to the initial conformation by minimizing the backbone RMSD to remove the effects of global rotation. In two simulations of the Ala44:NC(35−50) peptide, there are relatively small changes in the RMSD as a function of time, suggesting that the introduction of the mutation does not strongly perturb the native structure of the peptide. This is reasonable since we are replacing a more bulky group, His, by a less bulky group, Ala. In the third simulation of Ala44:NC(35−50), there are more significant conformational changes as measured by the increase in RMSD to over 3 Å. Two structural transitions occur during the simulation, notably at 2 and 4 ns. Both transitions involve changes in backbone conformation of residues 43−47, which undergo a small change in conformation during the first transition, followed by more significant conformational changes in the second. Clustering the struc-

tures from these three simulations using the criteria specified in the methods section yielded seven cluster centers. In all simulations, the zinc ion remains bound to the peptide.

(b) Simulated Structures Are Consistent with NMR Data. The model of Ösapay and Case (*45*, *46*) was used to calculate the Hα chemical shifts from both the experimental and simulated structures of Ala44:NC(35−50). Good agreement with the experimental chemical shift data was found when using the experimental structures as indicated by the mean differences between the calculated and the experimental values for each residue (Figure 4B). Only the Hα of Thr50 shows a large deviation from the experimental value. This is likely due to a large degree of conformational flexibility of this C-terminal residue that is not extensively sampled in the family of NMR structures. The RMSD between the calculated and the experimental chemical shifts for the experimental structures was 0.4 ppm; however, if the Thr50 Hα is excluded, the value is 0.3 ppm. Other residues that also show deviations that exceed the accuracy of the model (0.2 ppm) are the Hα protons of Trp37 and Lys38. The chemical shifts calculated using the structures from the molecular dynamics simulations are in better agreement with the experimental chemical shifts than the chemical shifts calculated from the experimental NMR structures (Figure 4B); the average RMSD for all Hα protons was 0.21 ppm. As with the NMR structures, larger deviations from the experimental values were observed for the Trp37 and Lys38 residues, suggesting insufficient sampling of the aromatic ring conformation.

Interproton distances for proton pairs corresponding to the experimental NOEs were calculated from the molecular dynamics simulations. These were compared to the upper and lower bounds of the NOEs restraints used in the structure determination; the comparison was made between protons belonging to residues separated by more than one residue (i, $i \pm x$; $x > 1$). Overall, the results are satisfactory as there are only a few violations of the long-range NOEs; in one of the simulations, there were four violations, and in the other two simulations only three violations were found. In all three simulations, two violations involved the pair between the Hα of Thr50 and the side chain Hζ2 of Trp37 and the pair between the Hβ proton of Asp48 and the Hδ1 proton of Trp37. This suggests that the simulations are probably not sufficiently long to sample all the possible rotamers of Trp37.

(c) Larger Atomic Fluctuations Are Observed in the Vicinity of the Point Mutation. The atomic fluctuations were calculated and averaged by residue for every 25 ps segment of the molecular dynamics trajectories. Each structure was reoriented relative to the backbone atoms of residues 36:41 and 48:50 to remove global rotation. An overall average value was calculated, and the results are shown in Figure 5. The most flexible part of the peptide is found in the region of the His44 mutation, while the N- and C-termini of the peptide are less flexible than the region around the mutation. This is consistent with the experimental structures where the most structurally variable region of the peptide is around the His44 mutation and the least variable region is the N-terminal end of the peptide. This increased flexibility in the region of the mutation explains why fewer long-range NOEs involving residues in this region of the peptide are observed experimentally.

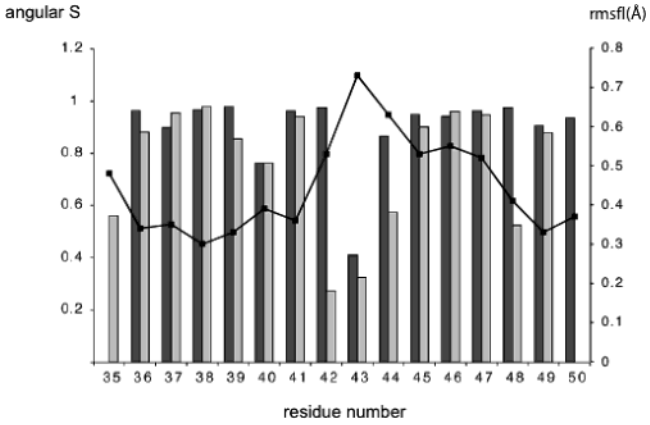

FIGURE 5: Angular order parameter *S* and RMS fluctuations as a function of sequence for the simulation structures. Angular order parameters *S* were calculated for psi (light gray bars) and phi (dark gray bars) Ala44:NC(35−50) angles. An *S* value close to zero means that the angle distribution in the structure ensemble is random, whereas an *S* value equal to 1 characterizes a rigid torsion angle. The black curve indicates the average RMS fluctuations from the ensemble of Ala44:NC(35−50) structures from the simulations after superposition of residues Gly35−Lys41 and Asp48−Thr50. The RMS fluctuations were calculated for the backbone atoms only.

Using the ensemble of average structures from the simulations, we calculated the dihedral angle order parameter (*S*) for the backbone dihedral angles. These results show that in the vicinity of the mutation, where the larger backbone RMS fluctuations were observed, the order parameter is decreased corresponding to a greater variation in the backbone dihedral angles. Dihedral angles are internal coordinates, and they are, therefore, independent of the global reorientation used in calculating the average structures and the RMS fluctuations. The variation of *S* along the peptide chain resembles that observed for the experimental structures; however, in the case of the experimental structures, there is a greater dispersion of values. This is probably because the ensemble of NMR structures samples a greater range of conformational space than that sampled by the simulations. Conformational exchange in the more stable region of the protein is likely to occur on a time scale longer than the time scale of the simulations.

(d) Zinc Binding and Local Unfolding. The molecular dynamics simulations of Ala44:NC(35−50) provide further proof that the mutant peptide is able to bind zinc ion. In all three simulations, which started from different initial structures and conditions, zinc remained bound to the peptide via the three Cys residues. Analysis of the zinc binding site during the molecular dynamics simulations suggests several possible mechanisms. These are illustrated by the structures presented in Figure 6, which present two structures of Ala44:NC(35−50), one in which the peptide is near the native conformation and one in which the peptide backbone is more than 3.0 Å RMSD from the native structure. In the former case (Figure 6A), the average structure shows that the backbone carbonyl oxygen atoms reorient toward the zinc ion and provide a favorable electrostatic environment to replace the fourth ligand. The relative distance between the zinc ion and the carbonyl oxygens decreased significantly over the course of the simulation to values as low as 4.2 Å while, at the same time, exhibited large fluctuations. This motion involves significant backbone motion, suggesting possible multiple conformations of the mutant zinc finger

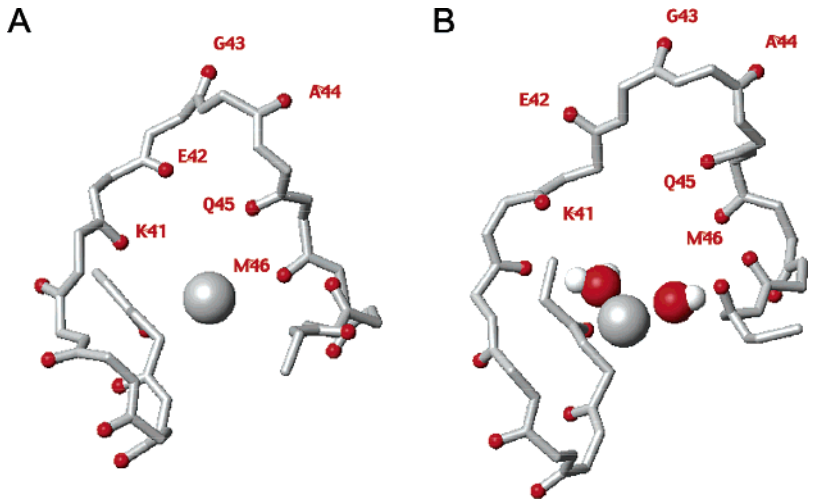

FIGURE 6: Average structures from the molecular dynamics simulations of the Ala44:NC(35−50) that illustrate the ligation of zinc in the mutant protein. In (A), the carbonyl oxygen atoms along the backbone reorient toward the zinc ion, while in a more unfolded protein (B) water molecules move into the first solvation shell of the zinc ion while making hydrogen bonds to the protein.

peptide in the vicinity of the mutated residue. In addition, the zinc ion undergoes a displacement in its position relative to the native peptide; this was also suggested by the NMR structures of Ala44:NC(35−50). In the simulation in which the peptide undergoes more significant conformational change and the Ala44 residue is further from the zinc binding site, water moves into the first solvation sphere of the ion and stabilizes the zinc binding by forming hydrogen bonds to neighboring residues (see Figure 6B). This is consistent with fluorescence studies, which suggest that a water molecule moves into the vacant ligand position (*36*).

Ala44:NC(35−50) Shows a Decreased DNA Binding Activity. In previous reports, it has been demonstrated that the binding site of NCp7 is approximately 5−7 nucleotides and that NCp7 shows a strong affinity for TG-rich oligonucleotides (*48*, *49*). For these reasons, $(TG)_3$ was selected as a representative target oligonucleotide. The binding process was monitored by following the intrinsic fluorescence of Trp37, since it has been shown that the fluorescence of Trp37 is strongly quenched due to stacking interactions with the G residues (*49*−*53*).

As expected, addition of increasing concentrations of $(TG)_3$ to a fixed concentration of NC(35−50) induced a large decrease of Trp37 fluorescence (Figure 7). Fitting the titration data with eq 3 provided an apparent binding constant, K_{obs}, of 3.0 (±0.3) × 10^4 M^{-1} and a maximum quenching extent of about 40%. The affinity of NC(35−50) for $(TG)_3$ was about 2 orders of magnitude smaller than the native protein one (*49*), confirming that the two finger motifs are required for high affinity (*54*).

By substituting NC(35−50) with Ala44:NC(35−50), a much smaller Trp37 fluorescence decrease was observed when $(TG)_3$ was added (Figure 7). For example, a 0.2 mM concentration of $(TG)_3$ decreased the fluorescence of Ala44:NC(35−50) by less than 5% as compared to about 40% in the case of NC(35−50)NC. This suggests either that Ala44:NC(35−50) binds to $(TG)_3$ with a very small affinity or alternatively that the binding of $(TG)_3$ does not affect Trp37 fluorescence in the mutated peptide. To discriminate between these two hypotheses, the fluorescence anisotropy of Ala44:NC(35−50) was measured in the presence of 0.3 mM $(TG)_3$ and compared to the fluorescence anisotropy of the peptide

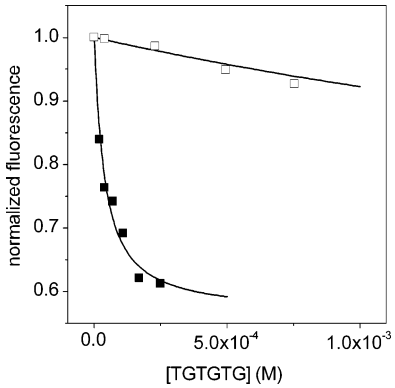

FIGURE 7: Binding of NC(35−50) and Ala44:NC(35−50) to $(TG)_3$. The concentration of NC(35−50) (filled squares) and Ala44:NC(35−50) (empty squares) was 9 μM. The solid lines represent the fits of the experimental points to eq 3 with the parameters given in the text.

in the absence of $(TG)_3$. Since the molecular weight of the $(TG)_3$/Ala44:NC(35−50) complex is more than twice that of the free peptide and since Trp37 fluorescence is almost unaffected in the presence of 0.3 mM $(TG)_3$, a significant increase in fluorescence anisotropy would be expected if the complex forms. In sharp contrast, we observed only a marginal change of the fluorescence anisotropy, strongly suggesting that only a small fraction of the Ala44:NC(35−50) molecules are complexed in the presence of 0.3 mM $(TG)_3$.

Because of the small Ala44:NC(35−50) fluorescence decrease in the tested concentration range of $(TG)_3$, an estimation of K_{obs} from Figure 7 is possible only if we fix the value of the fluorescence quenching that accompanies the complex formation. Assuming that formation of the $(TG)_3$/Ala44:NC(35−50) complex induces the same fluorescence decrease than with NC(35−50), we found that K_{obs} (≈200 M^{-1}) would be about two orders of magnitude lower than the NC(35−50) one.

DISCUSSION

In the present study, the structure of the C-terminal zinc finger motif of NCp7, Ala44:NC(35−50), where the native zinc-binding His residue has been mutated to an Ala residue

was investigated by NMR spectroscopy, molecular dynamics simulations, and fluorescence studies.

The NMR study performed at 274 K provides evidence that the three-dimensional structure of the N-terminal region of the mutant peptide is reminiscent of the wild type. The comparison of a peptide to the full-length protein in addressing the consequences of mutating of a zinc-binding residue is justified by the fact that HIV zinc finger motifs are independently folded domains (*6*). The lower temperature was necessary to narrow the NMR signals and permit ^{1}H signal assignment; at higher temperatures, the signals broadened indicating conformational exchange. The short and medium range NOE pattern observed for Ala44:NC(35−50) and the one published for the wild type domain within a larger construct containing the two zinc binding domains of NCp7 (*6*, *55*) are similar in the region spanning Gly35 to Gly40. This demonstrates that the loss of the zinc coordinating His residue does not affect the N-terminal part of the zinc binding domain. Moreover, the orientation of the three remaining Cys residues suggests that the mutant peptide continues to bind zinc ion. Replacing His 44 by an Ala had a dramatic effect on the structure and dynamics of the peptide in the vicinity of the mutation. Slow conformational exchange led to a poorly defined solution structure of the peptide in this region. The NMR data also showed that the conformation of the C-terminal part of the mutant differed significantly from that of the native structure in the region of residues 44−49, where the NMR studies suggest a local unfolding of the peptide.

Comparison of the structures from the simulations to the native structure indicates that most of the conformational changes are limited to the vicinity around the His-to-Ala mutation. The simulation results confirm that the mutation of the native His 44 to an Ala has little effect on the structure of the N-terminal end of the peptide, since in all simulations it remains close to the native structure. The simulations also confirm that the mutation significantly perturbs the structure of the peptide in the region of residues 44−49. In this region of the peptide, the simulations predict large-scale conformational changes that lead to a local unfolding.

Substitution of His44 by Ala reduces the binding constant of this mutant for Zn^{2+} relative to the native peptide (*36*). From the molecular dynamics simulations, a structural model emerges for zinc binding by the mutant peptide. The conformational changes associated with the mutation, in part, compensate for the loss of the zinc-coordinating interactions due to the mutation. The conformational changes observed in the simulations include the reorientation of the backbone carbonyl oxygen atoms in the vicinity of the mutation to provide a favorable electrostatic environment that stabilizes the zinc ion. In addition, water molecules moved into the first solvation sphere of the zinc ion and made hydrogen bonds to the peptide further stabilizing the zinc ion binding. The entry of water into the peptide core upon unfolding has been observed in numerous protein unfolding simulations (*56*−*58*) and the exchange of a zinc-binding Cys for a water molecule has been observed in simulations of other zinc finger proteins (*59*). This suggests that zinc bound water may play an important role in the folding of zinc finger proteins by forming hydrogen bonds to the flexible polypeptide chain, reducing its mobility and allowing for the local rearrangements that are necessary to form the native structure.

A consequence of the structural changes due to the point mutation is the reorientation of certain amino acid side chains that are critical for nucleic acid binding. In the structure of native NCp7, a hydrophobic cleft is formed by residues Trp37, Gln45, and Met46 that belong to the oligonucleotide-binding site. In the structure of NCp7 complexed with ACGCC (*60*), Trp37 inserts between the C2 and G3 bases and stacks on the latter. Additional hydrophobic contacts are made by Gln45 and Met46 and involve the aromatic protons of C2, G3, and C4. In the NMR structures of the mutant peptide, as well as in the simulation structures, this hydrophobic cleft is not present. In every structure of the NMR ensemble, Gln45 and Met46 side chains were not found near Trp37 and in the simulated structures, the hydrophobic cleft is either structurally perturbed or not formed at all; the latter is particularly true for those structures in which local unfolding of the backbone occurred; see Figure 8A. To assess the possible consequences arising from these structural differences from the native conformation, a structure of Ala44(35−50)NCp7 Ala44:NC(35−50) determined by simulation was superimposed on the native NC(35−50) structure within the complex NC(12−53)-ACGCC (PDBID: 1BJ6, *60*); see Figure 8B. From this superposition, it is clearly shown that the side chains of Lys47, Met46, and Gln45 are in a different orientation relative to the native structure. The reorientation of these side chains strongly perturbs the formation of the hydrophobic cleft and thereby may reduce the affinity of the mutant peptide for nucleic acids. This hypothesis was checked by titrating both the wild-type NC-(35−50) peptide and the Ala44:NC(35−50) mutant with the model $(TG)_3$ oligonucleotide.

The change in the fluorescence properties of Trp37 demonstrated that the binding activity toward DNA of Ala44:NC(35−50) is strongly decreased relative to the native peptide and that only a small fraction of Ala44:NC(35−50) molecules are complexed to $(TG)_3$. The simulation results further suggest that two possible mechanisms of complexation to the $(TG)_3$ oligonucleotides are possible. The first is that Trp37 in the locally unfolded peptide continues to insert between the C2 and G3, but because Gln45 and Met46 are not in the good orientation for optimal binding, the additional hydrophobic contacts are lost and a reduced binding affinity is observed. A second possibility is based on the observation that near-native structures of Ala44:NC(35−50) were stable during the molecular dynamics simulations. Assuming that these conformations are accessible and populated, then it is the near-native conformation that interacts with the nucleic acid, although in a nonoptimal way.

The prevention of the hydrophobic cleft formation and the consequent decrease in the binding affinity of the distal finger motif for nucleic acids may well explain the dramatic decrease in viral RNA encapsidation when His44 was substituted by an Ala residue in viral particles (*15*). Interestingly, similar results were obtained when either His23 was substituted by a Cys residue (*31*, *61*) or when Cys28 was substituted by a His (*32*) in the proximal finger motif. Indeed, these mutations have been shown to not preclude the binding of zinc but to modify the side chain orientations of Val13, Phe16, Thr 24, and Ala25, preventing the formation on the N-terminal finger motif of the hydrophobic cleft for nucleic acid binding. This has been shown in turn to dramatically decrease the binding of the mutated protein to nucleic acids

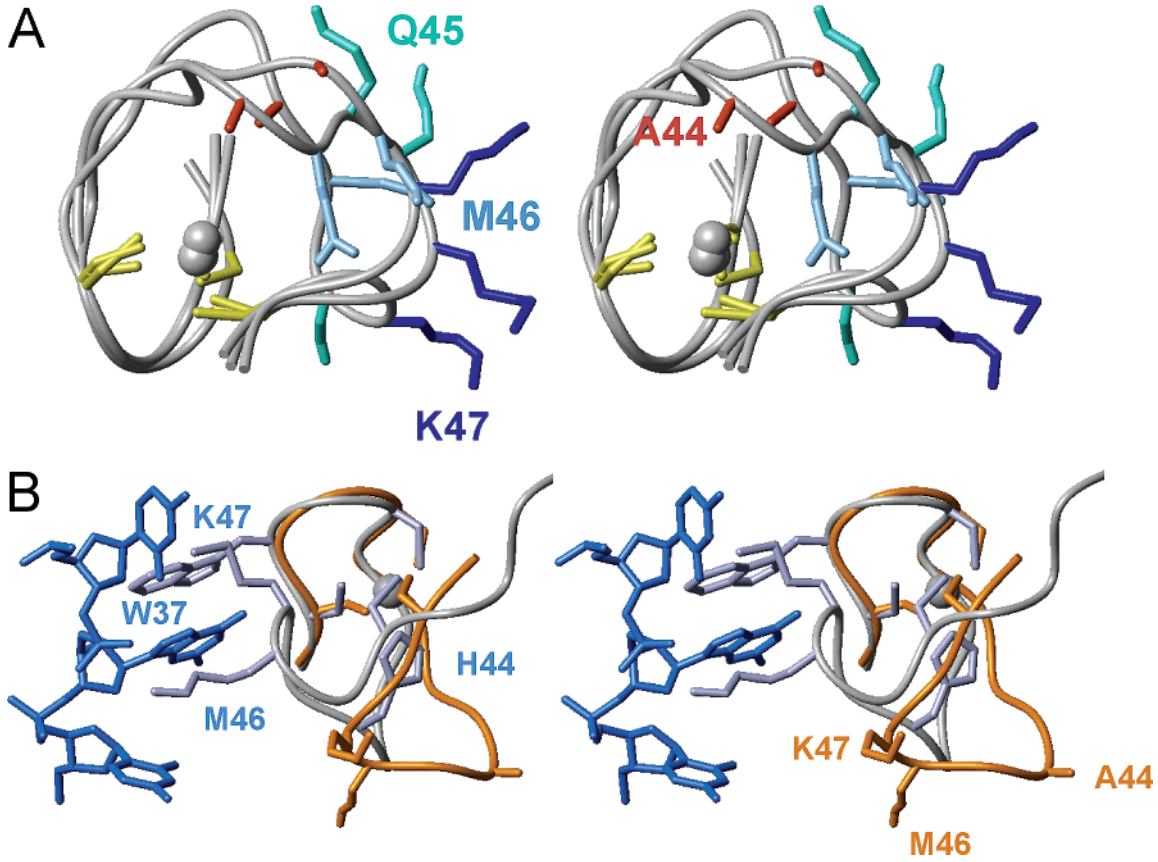

FIGURE 8: (A) Stereoview of three structures of the Ala44:NC(35−50) peptide from the molecular dynamics simulations that show the variation in orientation of side chains Gln45, Met46, and Lys47 due to changes in the backbone conformation. (B) Stereoview of Ala44:NC(35−50) superposed on the (35−50) sequence of the native NCp7 complexed to ACGCC. The backbone of the native peptide is shown in gray and that of the mutant peptide is shown in gold. Side chains of the native peptide are shown in gray (Trp37, His44, Met46, and Lys47); side chains of the mutant peptide are shown in gold (Ala44, Met46, and Lys47). For the sake of clarity, the orientation of the Trp 37 side chain was not shown for the mutant peptide.

and prevent efficient viral RNA recognition (*22*, *31*, *33*). It thus follows that in addition to the central role of the aromatic residues (Phe16 and Trp37) (*49*, *60*, *62*, *63*), the hydrophobic patches on both finger motifs are required for strong binding to nucleic acids. This may notably be critical for the proper recognition and selection of viral RNA among the cellular RNAs, which is thought to be achieved by Gag-NC molecules binding to the SL1, SL2, and SL3 domains of genomic RNA encapsidation sequence. This conclusion is in line with structural data on SL2/NCp7 (*63*) and SL3/NCp7 (*62*) complexes showing that these hydrophobic patches are involved in the binding of NCp7 to the loop sequences of both SL2 and SL3 domains.

However, since the reduction in RNA packaging in viruses with mutated NCp7 sequences is far less than the reduction in infectivity and since the reduction in RNA packaging for viruses with a His23 → Cys mutation in the NCp7 sequence (*22*) is under debate, this strongly suggests that the two hydrophobic patches may be involved in other NCp7 functions. A likely candidate would be NCp7 chaperone activity during the reverse transcription or integration steps. Indeed, it has been reported that the His23 → Cys mutation decreases the binding of NC to the TAR sequence involved in first stand transfer of the reverse transcription mechanism (*30*), impairs the chaperone activity of NCp7 during reverse transcription (*28*), and reduces the synthesis as well as the protection of complete proviral DNA (*33*, *34*). Similarly, the Cys28 → His mutation has been shown to induce a strong reduction of NCp7 chaperone activity during reverse transcription (*28*). Accordingly, it is suggested that the hydrophobic cleft formed by the hydrophobic patches on the two NCp7 finger motifs may constitute at least in part, the molecular support for NCp7 chaperone properties. Moreover, in addition to its effect on the hydrophobic patch, the His23 → Cys mutation results in a modification of the relative orientation of the two zinc finger motifs (*31*). The subsequent increase in the distance between both zinc fingers may additionally account for loss of activity. It is likely that the conformational changes afforded by the His44 → Ala mutation also disrupt the interaction between the two finger motifs and thus further contribute to an improper recognition of the nucleic acids targets and an impaired NCp7 activity on them.

Together with previous data, our results highlight the importance of the limited conformational space imposed by the four highly conserved zinc coordinating residues in each HIV-1 zinc finger motif. It appears that the highly folded and constrained backbone structure imposed by the coordination of the four zinc coordinates to zinc in both finger motifs is required for providing a proper orientation of the hydrophobic and aromatic residues that form the interacting surface with the nucleic acid targets. It is also likely that the proper orientation of the surface residues contribute to keep the fingers in close proximity to optimize the interacting surface.

ACKNOWLEDGMENT

Claude Ling is acknowledged for his technical support and Patrice Petitjean for the synthesis of the mutant protein. Supercomputer time was provided by a grant from the Centre Informatique National de l'Enseignement Supérieur (CINES) and from the Institut du Développement et des Ressources en Informatique Scientifique (IDRIS).

REFERENCES

1. Maurer, B., Bannert, H., Darai, G., and Flugel, R. M. (1988) Analysis of the primary structure of the long terminal repeat and the gag and pol genes of the human spumaretrovirus, *J. Virol. 62*, 1590−1597.
2. Maurer, B., and Flugel, R. M. (1988) Genomic organization of the human spumaretrovirus and its relatedness to AIDS and other retroviruses, *AIDS Res. Hum. Retroviruses 4*, 467−473.
3. Berg, J. M. (1986) Potential metal-binding domains in nucleic acid binding proteins, *Science 232*, 485−487.
4. Mely, Y., De Rocquigny, H., Morellet, N., Roques, B. P., and Gerard, D. (1996) Zinc binding to the HIV-1 nucleocapsid protein: a thermodynamic investigation by fluorescence spectroscopy, *Biochemistry 35*, 5175−5182.
5. Bombarda, E., Morellet, N., Cherradi, H., Spiess, B., Bouaziz, S., Grell, E., Roques, B. P., and Mely, Y. (2001) Determination of the pKa of the four Zn^{2+}-coordinating residues of the distal finger motif of the HIV-1 nucleocapsid protein: consequences on the binding of Zn2+, *J. Mol. Biol. 310*, 659−672.
6. Summers, M. F., Henderson, L. E., Chance, M. R., Bess, J. W., Jr., South, T. L., Blake, P. R., Sagi, I., Perez-Alvarado, G., and Sowder et al. (1992) Nucleocapsid zinc fingers detected in retroviruses: EXAFS studies of intact viruses and the solution-state structure of the nucleocapsid protein from HIV-1, *Protein Sci. 1*, 563−574.
7. Morellet, N., Jullian, N., De Rocquigny, H., Maigret, B., Darlix, J. L., and Roques, B. P. (1992) Determination of the structure of the nucleocapsid protein NCp7 from the human immunodeficiency virus type 1 by 1H NMR, *EMBO J. 11*, 3059−3065.
8. Morellet, N., de Rocquigny, H., Mely, Y., Jullian, N., Demene, H., Ottmann, M., Gerard, D., Darlix, J. L., Fournie-Zaluski, M. C., and Roques, B. P. (1994) Conformational behaviour of the active and inactive forms of the nucleocapsid NCp7 of HIV-1 studied by 1H NMR, *J. Mol. Biol. 235*, 287−301.
9. Mely, Y., Jullian, N., Morellet, N., De Rocquigny, H., Dong, C. Z., Piemont, E., Roques, B. P., and Gerard, D. (1994) Spatial proximity of the HIV-1 nucleocapsid protein zinc fingers investigated by time-resolved fluorescence and fluorescence resonance energy transfer, *Biochemistry 33*, 12085−12091.
10. Lee, B. M., De Guzman, R. N., Turner, B. G., Tjandra, N., and Summers, M. F. (1998) Dynamical behavior of the HIV-1 nucleocapsid protein, *J. Mol. Biol. 279*, 633−649.
11. Chertova, E. N., Kane, B. P., McGrath, C., Johnson, D. G., Sowder, R. C., 2nd, Arthur, L. O., and Henderson, L. E. (1998) Probing the topography of HIV-1 nucleocapsid protein with the alkylating agent *N*-ethylmaleimide, *Biochemistry 37*, 17890−17897.
12. Scozzafava, A., Mastrolorenzo, A., and Supuran, C. T. (2001) Agents that target cysteine residues of biomolecules and their therapeutic potential, *Exp. Opin. Ther. Pat. 11*, 765−787.
13. Aldovini, A., and Young, R. A. (1990) Mutations of RNA and protein sequences involved in human immunodeficiency virus type 1 packaging result in production of noninfectious virus, *J. Virol. 64*, 1920−1926.
14. Gorelick, R. J., Nigida, S. M., Jr., Bess, J. W., Jr., Arthur, L. O., Henderson, L. E., and Rein, A. (1990) Noninfectious human immunodeficiency virus type 1 mutants deficient in genomic RNA, *J. Virol. 64*, 3207−3211.
15. Dorfman, T., Luban, J., Goff, S. P., Haseltine, W. A., and Gottlinger, H. G. (1993) Mapping of functionally important residues of a cysteine-histidine box in the human immunodeficiency virus type 1 nucleocapsid protein, *J. Virol. 67*, 6159−6169.
16. Zhang, Y., and Barklis, E. (1995) Nucleocapsid protein effects on the specificity of retrovirus RNA encapsidation, *J. Virol. 69*, 5716−5722.
17. Schwartz, M. D., Fiore, D., and Panganiban, A. T. (1997) Distinct functions and requirements for the Cys-His boxes of the human immunodeficiency virus type 1 nucleocapsid protein during RNA encapsidation and replication, *J. Virol. 71*, 9295−9305.
18. Dupraz, P., Oertle, S., Meric, C., Damay, P., and Spahr, P. F. (1990) Point mutations in the proximal Cys-His box of Rous sarcoma virus nucleocapsid protein, *J. Virol. 64*, 4978−4987.
19. Dupraz, P., and Spahr, P. F. (1993) Analysis of deletions and thermosensitive mutations in Rous sarcoma virus gag protein p10, *J. Virol. 67*, 3826−3834.
20. Berkowitz, R., Fisher, J., and Goff, S. P. (1996) RNA packaging, *Curr. Top. Microbiol. Immunol. 214*, 177−218.
21. Gorelick, R. J., Chabot, D. J., Ott, D. E., Gagliardi, T. D., Rein, A., Henderson, L. E., and Arthur, L. O. (1996) Genetic analysis of the zinc finger in the Moloney murine leukemia virus nucleocapsid domain: replacement of zinc-coordinating residues with other zinc-coordinating residues yields noninfectious particles containing genomic RNA, *J. Virol. 70*, 2593−2597.
22. Gorelick, R. J., Gagliardi, T. D., Bosche, W. J., Wiltrout, T. A., Coren, L. V., Chabot, D. J., Lifson, J. D., Henderson, L. E., and Arthur, L. O. (1999) Strict conservation of the retroviral nucleocapsid protein zinc finger is strongly influenced by its role in viral infection processes: characterization of HIV-1 particles containing mutant nucleocapsid zinc-coordinating sequences, *Virology 256*, 92−104.
23. Remy, E., de Rocquigny, H., Petitjean, P., Muriaux, D., Theilleux, V., Paoletti, J., and Roques, B. P. (1998) The annealing of tRNA3Lys to human immunodeficiency virus type 1 primer binding site is critically dependent on the NCp7 zinc fingers structure, *J. Biol. Chem. 273*, 4819−4822.
24. Rong, L., Liang, C., Hsu, M., Kleiman, L., Petitjean, P., de Rocquigny, H., Roques, B. P., and Wainberg, M. A. (1998) Roles of the human immunodeficiency virus type 1 nucleocapsid protein in annealing and initiation versus elongation in reverse transcription of viral negative-strand strong-stop DNA, *J. Virol. 72*, 9353−9358.
25. Guo, J., Wu, T., Anderson, J., Kane, B. F., Johnson, D. G., Gorelick, R. J., Henderson, L. E., and Levin, J. G. (2000) Zinc finger structures in the human immunodeficiency virus type 1 nucleocapsid protein facilitate efficient minus- and plus-strand transfer, *J. Virol. 74*, 8980−8988.
26. Williams, M. C., Rouzina, I., Wenner, J. R., Gorelick, R. J., Musier-Forsyth, K., and Bloomfield, V. A. (2001) Mechanism for nucleic acid chaperone activity of HIV-1 nucleocapsid protein revealed by single molecule stretching, *Proc. Natl. Acad. Sci. U.S.A. 98*, 6121−6126.
27. Bernacchi, S., Stoylov, S., Piemont, E., Ficheux, D., Roques, B. P., Darlix, J. L., and Mely, Y. (2002) HIV-1 nucleocapsid protein activates transient melting of least stable parts of the secondary structure of TAR and its complementary sequence, *J. Mol. Biol. 317*, 385−399.
28. Guo, J., Wu, T., Kane, B. F., Johnson, D. G., Henderson, L. E., Gorelick, R. J., and Levin, J. G. (2002) Subtle alterations of the native zinc finger structures have dramatic effects on the nucleic acid chaperone activity of human immunodeficiency virus type 1 nucleocapsid protein, *J. Virol. 76*, 4370−4378.
29. Heath, M. J., Derebail, S. S., Gorelick, R. J., and DeStefano, J. J. (2003) Differing roles of the N- and C-terminal zinc fingers in human immunodeficiency virus nucleocapsid protein-enhanced nucleic acid annealing, *J. Biol. Chem. 278*, 30755−30763.
30. Lee, N., Gorelick, R. J., and Musier-Forsyth, K. (2003) Zinc finger-dependent HIV-1 nucleocapsid protein-TAR RNA interactions, *Nucleic Acids Res. 31*, 4847−4855.
31. Demene, H., Dong, C. Z., Ottmann, M., Rouyez, M. C., Jullian, N., Morellet, N., Mely, Y., Darlix, J. L., Fournie-Zaluski, M. C., and Saragosti et, a. (1994) 1H NMR structure and biological studies of the His23→Cys mutant nucleocapsid protein of HIV-1 indicate that the conformation of the first zinc finger is critical for virus infectivity, *Biochemistry 33*, 11707−11716.
32. Ramboarina, S., Morellet, N., Fournie-Zaluski, M. C., Roques, B. P., and Moreller, N. (1999) Structural investigation on the requirement of CCHH zinc finger type in nucleocapsid protein of human immunodeficiency virus 1, *Biochemistry 38*, 9600−9607.
33. Tanchou, V., Decimo, D., Pechoux, C., Lener, D., Rogemond, V., Berthoux, L., Ottmann, M., and Darlix, J. L. (1998) Role of the N-terminal zinc finger of human immunodeficiency virus type 1 nucleocapsid protein in virus structure and replication, *J. Virol. 72*, 4442−4447.
34. Buckman, J. S., Bosche, W. J., and Gorelick, R. J. (2003) Human immunodeficiency virus type 1 nucleocapsid Zn^{2+} fingers are

required for efficient reverse transcription, initial integration processes, and protection of newly synthesized viral DNA, *J. Virol. 77*, 1469−1480.
35. Williams, M. C., Rouzina, I., and Bloomfield, V. A. (2002) Thermodynamics of DNA interactions from single molecule stretching experiments, *Acc. Chem. Res. 35*, 159−166.
36. Bombarda, E., Cherradi, H., Morellet, N., Roques, B. P., and Mely, Y. (2002) Zn^{2+} binding properties of single-point mutants of the C-terminal zinc finger of the HIV-1 nucleocapsid protein: evidence of a critical role of cysteine 49 in Zn^{2+} dissociation, *Biochemistry 41*, 4312−4320.
37. de Rocquigny, H., Ficheux, D., Gabus, C., Fournie-Zaluski, M. C., Darlix, J. L., and Roques, B. P. (1991) First large scale chemical synthesis of the 72 amino acid HIV-1 nucleocapsid protein NCp7 in an active form, *Biochem. Biophys. Res. Commun. 180*, 1010−1018.
38. Piotto, M., Saudek, V., and Sklenar, V. (1992) Gradient-tailored excitation for single-quantum NMR spectroscopy of aqueous solutions, *J. Biomol. NMR 2*, 661−665.
39. Bartels, C., Xia, T.-h., and Wuthrich, K. (1993) The program xeasy for computer-supported NMR spectral analysis in the three-dimensional structure determination of biomacromolecules, *J. Mol. Graphics 11*, 263.
40. Brunger, A. T. (1992) X-PLOR, Version 3.1. A System for X-ray Crystallography and NMR, Yale University Press, New Haven, CT.
41. Nilges, M., Clore, G. M., and Gronenborn, A. M. (1988) Determination of three-dimensional structures of proteins from interproton distance data by dynamical simulated annealing from a random array of atoms Circumventing problems associated with folding, *FEBS Lett. 239*, 129−136.
42. Koradi, R., Billeter, M., and Wuthrich, K. (1996) MOLMOL: a program for display and analysis of macromolecular structures, *J. Mol. Graphics 14*, 51−5, 29−32.
43. Brooks, B. R., Bruccoleri, R. E., Olafson, B. D., States, D. J., Swaminathan, S., and Karplus, M. J. (1983) CHARMM: A program for macromolecular energy minimization and dynamics calculations, *J. Comput. Chem. 4*, 187−217.
44. MacKerell, A. D. J., Bashford, D., Bellott, M., Dunbrack, R. L. J., Evanseck, J. D., Field, M. J., Fischer, S., Gao, J., Guo, H., Ha, S., Joseph-McCarthy, D., Kuchnir, L., Kuczera, K., Lau, F. T. K., Mattos, C., Michnick, S., Ngo, T., Nguyen, D. T., Prodhom, B., Reiher, W. E. I., Roux, B., Schlenkrich, M., Smith, J. C., Stote, R., Straub, J., Watanabe, M., Wiorkiewicz-Kuczera, J., Yin, D., and Karplus, M. (1998) All-atom empirical potential for molecular modeling and dynamics studies of proteins, *J. Phys. Chem. 102*, 3586−3616.
45. Osapay, C., and Case, D. A. (1991) A new analysis of proton chemical shifts in proteins, *J. Am. Chem. Soc. 113*, 9436−9444.
46. Osapay, K., and Case, D. A. (1994) Analysis of proton chemical shifts in regular secondary structure of proteins, *J. Biomol. NMR 4*, 215−230.
47. Karpen, M. E., Tobias, D. J., and Brooks, C. L., 3rd. (1993) Statistical clustering techniques for the analysis of long molecular dynamics trajectories: analysis of 2.2-ns trajectories of YPGDV, *Biochemistry 32*, 412−420.
48. Fisher, R. J., Rein, A., Fivash, M., Urbaneja, M. A., Casas-Finet, J. R., Medaglia, M., and Henderson, L. E. (1998) Sequence-specific binding of human immunodeficiency virus type 1 nucleocapsid protein to short oligonucleotides, *J. Virol. 72*, 1902−1909.
49. Vuilleumier, C., Bombarda, E., Morellet, N., Gerard, D., Roques, B. P., and Mely, Y. (1999) Nucleic acid sequence discrimination by the HIV-1 nucleocapsid protein NCp7: a fluorescence study, *Biochemistry 38*, 16816−16825.
50. Mely, Y., Piemont, E., Sorinas-Jimeno, M., de Rocquigny, H., Jullian, N., Morellet, N., Roques, B. P., and Gerard, D. (1993) Structural and dynamic characterization of the aromatic amino acids of the human immunodeficiency virus type I nucleocapsid protein zinc fingers and their involvement in heterologous tRNA-(Phe) binding: a steady-state and time-resolved fluorescence study, *Biophys. J. 65*, 1513−1522.
51. Bombarda, E., Ababou, A., Vuilleumier, C., Gerard, D., Roques, B. P., Piemont, E., and Mely, Y. (1999) Time-resolved fluorescence investigation of the human immunodeficiency virus type 1 nucleocapsid protein: influence of the binding of nucleic acids, *Biophys. J. 76*, 1561−1570.
52. Maki, A. H., Ozarowski, A., Misra, A., Urbaneja, M. A., and Casas-Finet, J. R. (2001) Phosphorescence and optically detected magnetic resonance of HIV-1 nucleocapsid protein complexes with stem-loop sequences of the genomic Psi-recognition element, *Biochemistry 40*, 1403−1412.
53. Shubsda, M. F., Paoletti, A. C., Hudson, B. S., and Borer, P. N. (2002) Affinities of packaging domain loops in HIV-1 RNA for the nucleocapsid protein, *Biochemistry 41*, 5276−5282.
54. Urbaneja, M. A., Kane, B. P., Johnson, D. G., Gorelick, R. J., Henderson, L. E., and Casas-Finet, J. R. (1999) Binding properties of the human immunodeficiency virus type 1 nucleocapsid protein p7 to a model RNA: elucidation of the structural determinants for function, *J. Mol. Biol. 287*, 59−75.
55. Omichinski, J. G., Clore, G. M., Sakaguchi, K., Appella, E., and Gronenborn, A. M. (1991) Structural characterization of a 39-residue synthetic peptide containing the two zinc binding domains from the HIV-1 p7 nucleocapsid protein by CD and NMR spectroscopy, *FEBS Lett. 292*, 25−30.
56. Daggett, V., and Levitt, M. (1993) Protein unfolding pathways explored through molecular dynamics simulations, *J. Mol. Biol. 232*, 600−619.
57. Caflisch, A., and Karplus, M. (1994) Molecular dynamics simulation of protein denaturation: solvation of the hydrophobic cores and secondary structure of barnase, *Proc. Natl. Acad. Sci. U.S.A. 91*, 1746−1750.
58. Marti-Renom, M. A., Stote, R. H., Querol, E., Aviles, F. X., and Karplus, M. (1998) Refolding of potato carboxypeptidase inhibitor by molecular dynamics simulations with disulfide bond constraints, *J. Mol. Biol. 284*, 145−172.
59. Bredenberg, J., and Nilsson, L. (2002) Conformational states of the glucocorticoid receptor DNA-binding domain from molecular dynamics simulations, *Proteins 49*, 24−36.
60. Morellet, N., Demene, H., Teilleux, V., Huynh-Dinh, T., de Rocquigny, H., Fournie-Zaluski, M. C., and Roques, B. P. (1998) Structure of the complex between the HIV-1 nucleocapsid protein NCp7 and the single-stranded pentanucleotide d(ACGCC), *J. Mol. Biol. 283*, 419−434.
61. Julian, N., Demene, H., Morellet, N., Maigret, B., and Roques, B. P. (1993) Replacement of His23 by Cys in a zinc finger of HIV-1 NCp7 led to a change in 1H NMR-derived 3D structure and to a loss of biological activity, *FEBS Lett. 331*, 43−48.
62. De Guzman, R. N., Wu, Z. R., Stalling, C. C., Pappalardo, L., Borer, P. N., and Summers, M. F. (1998) Structure of the HIV-1 nucleocapsid protein bound to the SL3 psi-RNA recognition element, *Science 279*, 384−388.
63. Amarasinghe, G. K., De Guzman, R. N., Turner, R. B., Chancellor, K. J., Wu, Z. R., and Summers, M. F. (2000) NMR structure of the HIV-1 nucleocapsid protein bound to stem-loop SL2 of the psi-RNA packaging signal. Implications for genome recognition, *J. Mol. Biol. 301*, 491−511.

BI036137U